

# A Rydberg platform for non-ergodic chiral quantum dynamics

Riccardo J. Valencia-Tortora,<sup>1,\*</sup> Nicola Pancotti,<sup>2</sup> Michael Fleischhauer,<sup>3</sup> Hannes Bernien,<sup>4</sup> and Jamir Marino<sup>1</sup>

<sup>1</sup>*Institut für Physik, Johannes Gutenberg-Universität Mainz, D-55099 Mainz, Germany*

<sup>2</sup>*AWS Center for Quantum Computing, Pasadena, CA 91125, USA*

<sup>3</sup>*Department of Physics and Research Center OPTIMAS,*

*University of Kaiserslautern-Landau, D-67663 Kaiserslautern, Germany*

<sup>4</sup>*Pritzker School of Molecular Engineering, University of Chicago, Chicago, Illinois 60637, USA*

(Dated: September 25, 2023)

We propose a mechanism for engineering chiral interactions in Rydberg atoms via a *directional* antiblockade condition, where an atom can change its state only if an atom to its right (or left) is excited. The scalability of our scheme enables us to explore the many-body dynamics of kinetically constrained models with unidirectional character. We observe non-ergodic behavior via either scars, confinement, or localization, upon simply tuning the strength of two driving fields acting on the atoms. We discuss how our mechanism persists in the presence of classical noise and how the degree of chirality in the interactions can be tuned, providing paths for investigating a wide range of models.

*Introduction.*—Despite being far from full fault-tolerant quantum computing [1], reliable and versatile digital and analogue quantum simulations are nowadays attainable across a variety of atomic, molecular optical (AMO) as well as solid state platforms. Among the former, atomic Rydberg arrays stand out prominently due to their remarkable degree of programmability, as highlighted in various studies [2–6]. This has led to groundbreaking experiments in areas such as topological order [7, 8], engineerable quantum phase transitions [2, 3, 9, 10], lattice gauge theories [11], and strongly correlated quantum dynamics [2, 12–14]. Such broad flexibility suggests opportunities in designing quantum simulators without no direct counterpart in traditional AMO or condensed matter physics. In this context, a challenge centers on creating systems capable of demonstrating directionality, or more precisely non-reciprocal processes, that can differentiate, particularly in one dimension, between the flow of information in the right and left directions. The design of this class of quantum simulators is inspired from soft matter physics [15–17] and it would pave the way for the directional control of information flow in quantum networks and their associated quantum communication tasks [18].

In this work, we achieve this goal by presenting a blueprint for Rydberg atomic arrays featuring chiral interactions that aren't symmetric when neighboring atoms are exchanged. Specifically, we considered a one dimensional array with a staggered configuration of atomic positions and drive fields (cf. Fig. 1(a)). In such scenario, due to strong Van-der-Waals interactions we can access a regime we term *directional* antiblockade, wherein an atom can change its internal state solely when an atom to its right (or left) becomes excited. We first show that our mechanism is robust to experimental imperfections, like thermal disorder in atomic positions, and then simulate a variety of instances of directional kinetically constrained quantum models (KCMs). KCMs have attracted considerable interest due to their capability to display non-ergodic behavior despite their non-integrable and disorder-free character [15, 19–24]. In KCMs, slow-

down of thermalization could occur by means of various mechanisms: quantum scars [2, 25–30], where a few non-thermal excited states can lead to non-relaxing dynamics; confinement of quasi-particles induced by many-body interactions [11, 31–33]; or slow dynamics resulting from localization [19, 20]. These mechanisms are intricately linked to the specific constraints at play, and traditionally, each of them would necessitate a distinct experimental platform. Remarkably, in our Rydberg implementation, we can realize all of these mechanisms by simply adjusting the strength of the external drive fields. This versatility transforms our platform into a universal quantum simulator for non-ergodic quantum dynamics. As an additional benefit, our platform allows for the implementation of the quantum East model [19, 34], which has been absent in prior studies, albeit several Rydberg implementations have focused on related constrained models [35–41]. The significance of the quantum East model lies in its distinction as one of the rare cases where an interacting system undergoes a disorder-free transition between delocalization and localization in the ground state [19], which mirrors in a dynamical transition from slow to fast thermalization. It should be noted that this mechanism sets itself apart from other forms of ergodicity breaking, such as many-body localization (MBL), where the transition is attributed to the emergence of local conservation laws upon increasing disorder [42, 43]; Hilbert space shattering [44, 45], as the dynamics in the East model explores all states within the accessible Hilbert space albeit with varying connectivity; or Stark MBL [46–49], since East models exhibit translational invariance.

*Chiral interactions in Rydberg arrays.*—The key ingredient to engineer a directional interaction is a staggered configuration of the atomic spacings and drive fields in a Rydberg array (cf. Fig. 1(a)). The Hamiltonian describing such scenario, in the rotating frame with respect to

the bare atomic transitions, can be written as

$$\hat{H}(t) = \sum_{j=1}^N \left( \frac{1}{2} (\Omega_{1,j}(t) + \Omega_2(t)) \hat{\sigma}_j^+ + \text{H.c.} \right) + V_1 \sum_{j \text{ odd}} \hat{n}_j \hat{n}_{j+1} + V_2 \sum_{j \text{ even}} \hat{n}_j \hat{n}_{j+1} + V_{\text{NNN}} \sum_{j=1}^{N-2} \hat{n}_j \hat{n}_{j+2}, \quad (1)$$

where  $\hat{\sigma}_j^+ = |1\rangle_{jj}\langle 0|$  transfers the  $j$ -th atom from the ground state  $|0\rangle$  to the Rydberg state  $|1\rangle$ ;  $\hat{n}_j = |1\rangle_{jj}\langle 1|$ ;  $\Omega_{1,j}(t)$  and  $\Omega_2(t)$  are classical drive fields controllable in the experiment with Rabi frequencies  $\Omega_1$  and  $\Omega_2$ , respectively;  $V_1$  ( $V_2$ ) are Van-der-Waals interactions ( $V(r) = C_6/r^6$ ) on odd (even) bonds;  $V_{\text{NNN}}$  is the next-nearest neighbor interaction. Throughout, we work in the regime  $|V_{1,2}|, |V_1 - V_2| \gg \Omega_{1,2} \gg V_{\text{NNN}}$ . In this regime, interactions play a crucial role in dictating the dynamics of the single atom. Specifically, two extreme scenarios can be realized: excited atoms either inhibit spin-flips of neighboring ones (blockade) [50], or facilitate them (antiblockade) [51]. The blockade condition occurs by setting the drive field resonant with the bare atomic transitions so that the interaction energy due to a neighboring excited atom makes it off-resonant. Instead, the antiblockade occurs when the acting drive field is detuned from the bare atomic transitions by the interaction, and thus it becomes resonant solely if a neighboring atom is excited. In translational invariant systems, each atom cannot distinguish its right neighbor from the one to its left, and so no preferable direction can appear. In our scheme instead, since  $V_1 \neq V_2$ , the atom can distinguish the two neighboring atoms and we can selectively make processes resonant towards one direction and off-resonance towards the other. We term this mechanism *directional* antiblockade, which implies that an atom can flip only when an atom to its right (or left) is excited. In order to achieve this regime, it is enough to apply a single drive field on each atom, and so we temporarily set  $\Omega_2 = 0$ . A possible scheme is based on imprinting an additional staggered configuration in the drive field frequencies of  $\Omega_{1,j}(t)$ . Specifically, we can set the drive field on site  $j$  detuned by  $V_1$  (if  $j$  is even) or  $V_2$  (if  $j$  is odd) from the bare atomic transition, so that it is resonant solely when the atom to its left is excited and the one to its right is not, obtaining the anticipated *directional* antiblockade (see Fig. 1(b)). The net result is that an excitation seeded in the system triggers an avalanche of excitations solely towards ‘East’ (see Fig. 1(c)). In the Supplemental Material [52], we propose an alternative scheme where the staggered configuration is imprinted on the atomic frequencies, while instead the drive field is monochromatic.

*Experimental realization.*— In actual experiments, the *directional* antiblockade could be spoiled by finite temperature fluctuations, inhomogeneities due to the

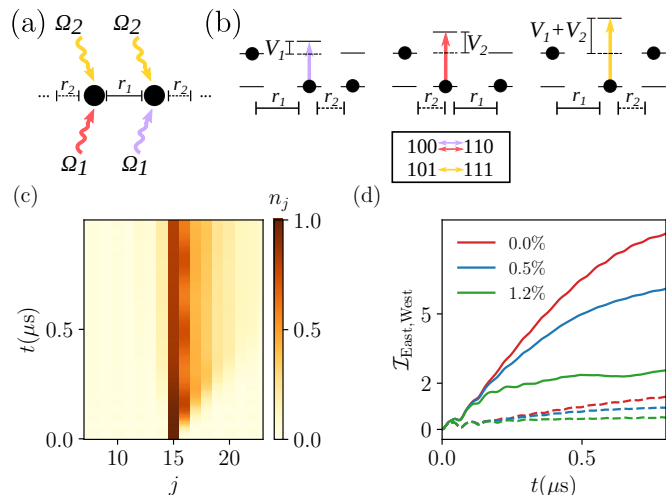


FIG. 1. (a): An array of Rydberg atoms in a staggered configuration of drive fields (each color refers to a different frequency) and spacings  $r_1$  and  $r_2$ , with corresponding nearest-neighbor interactions  $V_1$  and  $V_2$ . (b): Scheme of the most resonant processes (see box) which happen exclusively at the right of excited atoms due to the *directional* antiblockade. (c): Dynamics of the density profile seeding a single excitation and including thermal disorder in the atomic positions  $\tilde{\eta}_x = 0.012$  (see text). (d): Dynamics of the imbalances  $\mathcal{I}_{\text{East}}$  (continuous line) and  $\mathcal{I}_{\text{West}}$  (dashed line) starting from the same state as in (c) for different values of  $\tilde{\eta}_x$ . The imbalance  $\mathcal{I}_{\text{East}}$  ( $\mathcal{I}_{\text{West}}$ ) is defined as the sum of the average occupations to the right (left) of the initial seeded excitation. Excitations propagate preferably towards ‘East’ as desired ( $\mathcal{I}_{\text{East}} > \mathcal{I}_{\text{West}}$ ) despite finite temperature effects.

harmonic frequency trap holding the atoms, or dephasing coming from finite laser linewidth. The first two can be taken into account including quenched disorder in the atomic positions [53]. Specifically, at low enough temperature  $T$ , the displacements  $\delta \mathbf{r}_j$  from the ideal atomic positions are constant during a single experimental realization and distributed accordingly to a Gaussian distribution with zero average and width  $\eta_\alpha = \sqrt{k_B T / (m \omega_\alpha^2)}$  along the  $\alpha$ -axis, with  $\omega_\alpha$  the trapping frequency and  $m$  the atomic mass. Instead, dephasing induced by finite linewidth of the laser can be modelled by a Lindblad master equation with jump operators  $\hat{L}_j = \sqrt{\gamma} \hat{n}_j^z$ , with  $j \in [1, N]$ . Yet, in our setup we work in regimes where  $\gamma \sim 10$  kHz is at least two order of magnitudes smaller than the other energy scales, and therefore it can be neglected. Specifically, we will show results up to a time of  $10 \mu\text{s}$ , where the dynamics can be considered purely coherent as also spontaneous decay from the Rydberg state can be neglected. We elaborate further in the conclusions and Supplemental Material the opposite limit, where dephasing is large, illustrating how our scheme readily enables to investigate ‘classical’ non-ergodic dynamics with directional character. For concreteness, we consider  $^{87}\text{Rb}$  atoms located along the  $x$ -axis, at temperature  $T = 3 \mu\text{K}$  and optical traps with  $\omega_x = \omega_y = 5 \times \omega_z = 40$  kHz, which give rise to

an anisotropic disorder  $\eta_x = \eta_y = \eta_z/5 \approx 0.1 \mu\text{m}$ . We consider the atomic level  $70S$  as Rydberg state which has  $C_6/(2\pi) = 864 \text{ GHz}/(\mu\text{m})^6$ . In the following, we measure disorder as the relative variation with respect to the mean distance, namely  $\tilde{\eta}_\alpha \equiv \eta_\alpha/r_1$ . We consider Rabi frequencies  $\Omega_{1,2}$  in the range between  $2\pi \times 1 \text{ MHz}$  and  $2\pi \times 5 \text{ MHz}$ . For this set of parameters, we found as a good compromise between fast dynamics, small impact of disorder, and  $\Omega_{1,2} \ll V_{j,j+1}$ , the average spacings  $r_1 = 6.2 \mu\text{m}$  and  $r_2 = 5.4 \mu\text{m}$  (for which  $\tilde{\eta}_x \approx 0.01$ ), to which corresponds interactions  $V_1/(2\pi) = (15.0 \pm 1.0) \text{ MHz}$  and  $V_2/(2\pi) = (30.0 \pm 2.2) \text{ MHz}$ , respectively, and  $V_{\text{NNN}}/(2\pi) = (0.33 \pm 0.02) \text{ MHz}$ . Despite we show results mostly in this parameters' regime, we keep  $\tilde{\eta}_\alpha$  as a free parameter to explore different experimental scenarios. In the following, we show results averaged over 50 realizations of disorder, for which statistical errors are  $\sim 1\%$  or less. As it can be seen in Fig. 1(c-d), the main impact of disorder is a reduction of the propagating front, while its directional character is not appreciably spoiled. Having shown the robustness of our scheme, we now proceed on discussing some models immediately accessible by simply tuning the strength of the external drive fields.

*Kinetically constrained models.*— Before discussing the resulting dynamics of our scheme, we note that, using a single drive field, an atom remains frozen when both neighbors are excited. To enrich dynamics, we reintroduce the additional global drive field  $\Omega_2(t)$  with frequency detuned by  $V_1 + V_2$  from the bare atomic transition, so that it allows the transition  $|101\rangle \leftrightarrow |111\rangle$  (cf. Fig. 1(b)). As it is apparent, there is still no resonant process where an atom changes its state in the absence of an excited one to its left. In order to make it visible, we write down the following effective Hamiltonian describing the most resonant processes without taking into account disorder in the atomic positions (for further details see [52])

$$\hat{H} = \frac{1}{2} \sum_j \hat{n}_j \hat{\sigma}_{j+1}^x [\Omega_1 - (\Omega_1 - \Omega_2) \hat{n}_{j+2}] + \epsilon \sum_j \hat{n}_j + V_{\text{NNN}} \sum_j \hat{n}_j \hat{n}_{j+2}, \quad (2)$$

where we have introduced the detuning  $\epsilon$  from the perfect *directional* antiblockade which, together with  $V_{\text{NNN}}$ , can spoil the perfect resonance condition and inhibit spin-flips, as we will show later. The Hamiltonian in Eq. (2) belongs to the family of kinetically constrained quantum East models, where dynamics are activated solely to the right of excited sites. East models are characterized by a so-called ‘East symmetry’ [19], which implies that empty regions without any excitation to their left remain frozen. As a consequence, the location of the first excitation encountered starting from the left edge of the system does not change (see Fig. 1 (c)), and the Hilbert space splits in  $N$  disconnected sectors,

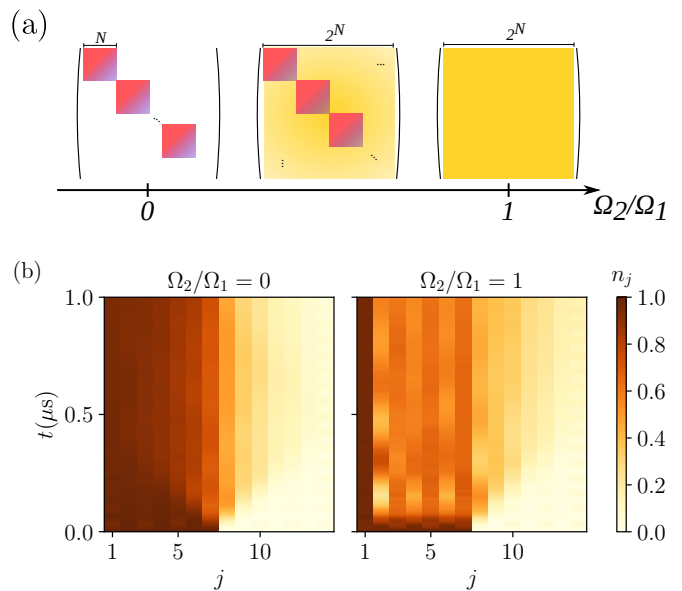


FIG. 2. (a) Sketch of the accessible Hilbert space, at fixed East symmetry sector, in a system of size  $N$  as a function of the Rabi frequencies  $\Omega_{1,2}$  (dynamics are initialized in product states). Colors indicate allowed transitions and they are in one-to-one correspondence with those used for the drive fields in Fig. 1(a). Blank spaces indicate forbidden transitions. For  $\Omega_1 \neq 0$  and  $\Omega_2 = 0$  strings of excitations can only shrink/expand without merging/splitting, leading to Hilbert space *shattering*; for  $\Omega_2/\Omega_1 \neq 0$ , strings achieve complete mobility, rendering the system ergodic, as any product state becomes accessible from any other. For  $\Omega_2/\Omega_1 = 1$  we recover the quantum East model [19, 34]. (b) Dynamics of the density profile starting from the product state with first half sites excited ( $|1\rangle$ ) and the rest in  $|0\rangle$  in the shattered ( $\Omega_2 = 0$ ) and ergodic regime ( $\Omega_{1,2} \neq 0$ ) including thermal disorder  $\tilde{\eta}_x = 0.012$  in units of the average spacing  $r_1 = 6.2 \mu\text{m}$ .

with  $N$  the system size. Once the East symmetry sector is specified by the location of the first excitation, we can further shape the accessible Hilbert space simply changing the relative power of the drive fields  $\Omega_1$  and  $\Omega_2$  (cf. Fig. 2(a)), which directly reflects in the mobility of excitations. Specifically, we will show that with a single drive field the East symmetry sector *shatters* in  $\mathcal{O}(e^N)$  disconnected sectors [45], while when both are active it is irreducible [19], meaning the dynamics connect all states (see Fig. 2). Then, we will illustrate the mechanisms by which in each regime the onset of thermalization considerably slows down within each irreducible sector, exhibiting scars, confinement, and localization. In the following, we discuss these three different regimes using the effective Hamiltonian in Eq. (2) as a guidance. Finally, we show how those features survive upon simulating the full theory [52] in Eq. (1).

*PXP model.*— For  $\Omega_1 = 0$  and  $\Omega_2 \neq 0$  directionality is lost and a spin flip occurs solely when both neighboring atoms are excited. This is reminiscent of the well-known

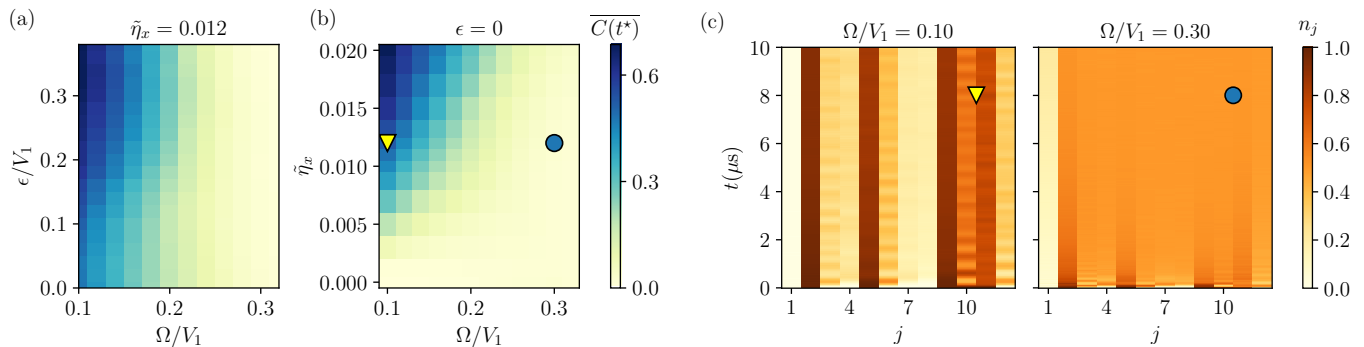


FIG. 3. Dynamics in the quantum East model of Refs. [19, 34] ( $\Omega_{1,2} = \Omega$ ) in the full theory (cf. Eq. (1)) initializing the state  $|01010001110\rangle$ . (a-b): Time-averaged autocorrelation function  $\overline{C(t^*)}$  at time  $t^* = 10\mu\text{s}$  keeping fixed either thermal disorder  $\tilde{\eta}_x$  or detuning  $\epsilon$ , respectively. For small  $\Omega$  the memory of the initial state is kept up to long times ( $\overline{C(t^*)} > 0$ ), while instead for large  $\Omega$  the memory of the initial state is rapidly washed out ( $\overline{C(t^*)} \approx 0$ ). (c): Dynamics of the density profile in the two phases (marked via symbols in (b)) at fixed thermal disorder  $\tilde{\eta}_x = 0.012$  in units of the average spacing  $r_1 = 6.2\mu\text{m}$  (see text).

PXP model, in which a spin flip occurs when both neighboring atoms are in the ground state. Indeed, the PXP model and ours share the same physics as they are connected via the transformation  $\hat{U} = \prod_{j=1}^N \hat{\sigma}_j^x$ , which translates to interchanging  $|0\rangle \leftrightarrow |1\rangle$ . This includes Hilbert space *shattering* [54] and the presence of quantum many-body scars, which slow down the onset of thermalization when initializing specific states (e.g. Néel state) [2, 26].

*Confinement.*— When  $\Omega_1 \neq 0$  and  $\Omega_2 = 0$ , strings of consecutive excitations can shrink or grow but not merge or split ( $|101\rangle \nleftrightarrow |111\rangle$ ), effectively experiencing a repulsive interaction. Additionally, the unidirectional character of the dynamics further reduces their mobility since the left edge of each string cannot move. Due to these constraints, each string of excitations is confined between its left edge and the left edge of the next one, and no entanglement can be generated between them during dynamics. As a result, the Hilbert space gets shattered in  $\mathcal{O}(e^N)$  disconnected sectors [45]. Since each string of excitations evolves independently from the others, we will focus on the largest irreducible sector containing a single string. We find that its dynamics are described by the Hamiltonian (for further details see [52])

$$\hat{H} = \frac{\Omega_1}{2} \sum_{k=1}^{N-1} (|k\rangle\langle k+1| + \text{H.c.}) + V_{\text{NNN}} \sum_{k=2}^N (k-2)|k\rangle\langle k|, \quad (3)$$

with  $|k\rangle \equiv |1\rangle^k |0\rangle^{N-k}$ , where the first term controls the change of the string length, while the second the potential energy proportional to such length. This Hamiltonian is integrable and has been derived in a number of similar scenarios [33, 55–57]. Direct inspection shows that Eq. (3) is the well-known hamiltonian of an electron in a lattice subjected to a constant electric field [56, 57]. Dynamics display Stark localization [56], which leads to real-time Bloch oscillations of period  $T_{\text{Bloch}} = 2\pi\Omega_1/V_{\text{NNN}}$  and size  $\ell_{\text{Bloch}} \sim \Omega_1/V_{\text{NNN}}$  originating from the right-

most edge of the string. Hence, excitations and quantum correlations are confined, preventing thermalization, closely resembling confinement in non-integrable systems [11, 31, 32, 58]. Upon introducing disorder, Bloch oscillations are still visible (see Fig. 2(b)) although partly suppressed.

*Quantum East model.*— When both drive fields are active ( $\Omega_{1,2} \neq 0$ ), strings of excitations gain full mobility since they can shrink, grow, merge, and split (cf. Fig. 2(b)). Thus, the accessible Hilbert space does not shatter and any product state can be dynamically reached by any other at fixed East symmetry sector [19]. Nonetheless, it is still possible to observe an extreme slowdown of thermalization. This can be immediately seen by setting  $\Omega_2/\Omega_1 = 1$ , for which Eq. (2) reduces to the quantum East model investigated in Refs. [19, 34] apart from additional density-density interactions which do not alter the qualitative picture. Such model has been shown to display a dynamical transition separating a fast and slow thermalizing phase [19, 34] due to the competing kinetic term  $\propto \Omega$  and on-site energy  $\propto \epsilon$ . Intuitively, if the kinetic term dominates ( $\Omega_{1,2}/(2\epsilon) \gtrsim 1$ ) strings of excitations expand and merge ballistically, fastly washing local information of the initial configuration, while if it is subleading ( $\Omega_{1,2}/(2\epsilon) \lesssim 1$ ), excitations can expand slowly, making possible to retrieve information about the initial conditions. Such behavior is strongly linked to the localization of the ground state and it can be observed for an exponentially large number, in the system size, of initial states [19]. Upon introducing thermal disorder  $\tilde{\eta}_\alpha$ , the picture is slightly affected. Indeed,  $\tilde{\eta}_\alpha$  can already induce undesired mismatches from the perfect resonant *directional* antiblockade condition. Thus, we expect the dynamics to be dictated by the competition of  $\Omega$  and the joint contribution of  $\tilde{\eta}_\alpha$  and  $\epsilon$ . We test this by initializing a representative highly-excited product state characterized by regions with low and high density of excitations. In the slow phase, heterogeneity in the initial state plays a crucial role in dictating the dynamics

up to very long times, in contrast with typical fast thermalizing systems where all local information is quickly lost except for global conserved quantities. We chose as proxy for distinguishing the different dynamical phases the autocorrelation function [15, 19]

$$C(t) = \frac{2}{Z} \sum_i \langle \hat{n}_i(t) \hat{n}_i(0) \rangle - 1, \quad (4)$$

where  $Z = \sum_i \langle \hat{n}_i(0) \rangle$  is a normalization constant. For the initial product state considered,  $C(t)$  is the density of the initially occupied sites at time  $t$ , to which we subtract an evenly distributed ‘background’ corresponding to an infinite temperature state,  $\langle n_i \rangle = 1/2$ . Thus,  $C(t)$  serves as a good proxy for memory of initial conditions, as its initial value is  $C(t=0) = 1$  and tends to zero when the system thermalizes. In Fig. 3(a-b) we show the time-average  $\overline{C(t^*)} = \int_0^{t^*} C(\tau) d\tau / t^*$  up to experimentally accessible time windows using the full theory (cf. Eq. (1)) in two scenarios: either keeping fixed the thermal disorder and varying  $\epsilon$ , or viceversa. As anticipated, both  $\epsilon$  and  $\tilde{\eta}_x$  contributes in slowing down dynamics. Indeed, in both dynamical phase diagrams we can distinguish a phase where the system retains memory of the initial state and a phase where the system fastly thermalizes and all local memory is quickly erased.

*Perspectives.*— In this work, we have proposed a scheme for realizing chiral interactions by means of a *directional* antiblockade condition, namely an atom can change its internal state only if the atom to its right (or left) is excited. Our scheme is based on ‘energetic’ arguments and gives rise to constrained interactions. Additionally, our protocol could be readily extended in presence of dominant classical noise. In such regime, dynamics is effectively described by rate equations, with rates dependent on the detunings, interactions and atomic configuration [35, 37], opening up to the simulation of dissipative uni-directional spin dynamics (for further details see [52]). Finally, we highlight that the degree of chirality in the interactions can be tuned by relaxing the condition  $\Delta V \equiv |V_1 - V_2| \gg \Omega$ . Specifically, for  $0 < \Delta V / \Omega \lesssim 1$ , dynamics still has a preferable direction, but there are near-resonant processes towards the other as well (similarly to other Rydberg proposals [59]). This offers a path for accessing regimes with a tunable *bias* towards one direction or the other. As an extreme example, in the zero *bias* case ( $\Delta V = 0$ ), and by setting  $\Omega_1 = \Omega_2/2$ , we can effectively simulate the quantum Fredrickson-Andersen model [60].

*Acknowledgements.*— This project has been supported by the Deutsche Forschungsgemeinschaft (DFG, German Research Foundation) through the Project ID 429529648-TRR 306 QuCoLiMa (“Quantum Cooperativity of Light and Matter”), and the grant HADEQUAM-MA7003/3-1; by the Dynamics and Topology Center, funded by the State of Rhineland Palatinate. This material is based

upon work supported by the US Department of Energy, Office of Science, National Quantum Information Science Research Centers. The work of M. F. has been supported by the DFG (SFB TR 185), project number 277625399. Parts of this research were conducted using the Mogon supercomputer and/or advisory services offered by Johannes Gutenberg University Mainz ([hpc.uni-mainz.de](http://hpc.uni-mainz.de)), which is a member of the AHRP (Alliance for High Performance Computing in Rhineland Palatinate, [www.ahrp.info](http://www.ahrp.info)), and the Gauss Alliance e.V. We gratefully acknowledge the computing time granted on the Mogon supercomputer at Johannes Gutenberg University Mainz ([hpc.uni-mainz.de](http://hpc.uni-mainz.de)) through the project “DysQ-Corr.”

---

\* Corresponding author: [rvalenci@uni-mainz.de](mailto:rvalenci@uni-mainz.de)

- [1] J. Preskill, Quantum computing in the NISQ era and beyond, *Quantum* **2**, 79 (2018).
- [2] H. Bernien, S. Schwartz, A. Keesling, H. Levine, A. Omran, H. Pichler, S. Choi, A. S. Zibrov, M. Endres, M. Greiner, V. Vuletić, and M. D. Lukin, Probing many-body dynamics on a 51-atom quantum simulator, *Nature* **551**, 579 (2017).
- [3] P. Scholl, M. Schuler, H. J. Williams, A. A. Eberharter, D. Barredo, K.-N. Schymik, V. Lienhard, L.-P. Henry, T. C. Lang, T. Lahaye, A. M. Läuchli, and A. Browaeys, Quantum simulation of 2d antiferromagnets with hundreds of rydberg atoms, *Nature* **595**, 233 (2021).
- [4] D. Bluvstein, A. Omran, H. Levine, A. Keesling, G. Semeghini, S. Ebadi, T. T. Wang, A. A. Michailidis, N. Maskara, W. W. Ho, S. Choi, M. Serbyn, M. Greiner, V. Vuletić, and M. D. Lukin, Controlling quantum many-body dynamics in driven rydberg atom arrays, *Science* **371**, 1355 (2021).
- [5] A. Browaeys and T. Lahaye, Many-body physics with individually controlled rydberg atoms, *Nature Physics* **16**, 132 (2020).
- [6] H. Labuhn, D. Barredo, S. Ravets, S. de Léséleuc, T. Macrì, T. Lahaye, and A. Browaeys, Tunable two-dimensional arrays of single rydberg atoms for realizing quantum ising models, *Nature* **534**, 667 (2016).
- [7] S. de Léséleuc, V. Lienhard, P. Scholl, D. Barredo, S. Weber, N. Lang, H. P. Büchler, T. Lahaye, and A. Browaeys, Observation of a symmetry-protected topological phase of interacting bosons with rydberg atoms, *Science* **365**, 775 (2019).
- [8] G. Semeghini, H. Levine, A. Keesling, S. Ebadi, T. T. Wang, D. Bluvstein, R. Verresen, H. Pichler, M. Kalinowski, R. Samajdar, A. Omran, S. Sachdev, A. Vishwanath, M. Greiner, V. Vuletić, and M. D. Lukin, Probing topological spin liquids on a programmable quantum simulator, *Science* **374**, 1242 (2021).
- [9] S. Ebadi, T. T. Wang, H. Levine, A. Keesling, G. Semeghini, A. Omran, D. Bluvstein, R. Samajdar, H. Pichler, W. W. Ho, S. Choi, S. Sachdev, M. Greiner, V. Vuletić, and M. D. Lukin, Quantum phases of matter on a 256-atom programmable quantum simulator, *Nature* **595**, 227 (2021).
- [10] A. Keesling, A. Omran, H. Levine, H. Bernien, H. Pichler, S. Choi, R. Samajdar, S. Schwartz, P. Silvi,

- S. Sachdev, P. Zoller, M. Endres, M. Greiner, V. Vuletić, and M. D. Lukin, Quantum kibble–zurek mechanism and critical dynamics on a programmable rydberg simulator, *Nature* **568**, 207 (2019).
- [11] F. M. Surace, P. P. Mazza, G. Giudici, A. Lerose, A. Gambassi, and M. Dalmonte, Lattice gauge theories and string dynamics in rydberg atom quantum simulators, *Phys. Rev. X* **10**, 021041 (2020).
- [12] V. Lienhard, S. de Léséleuc, D. Barredo, T. Lahaye, A. Browaeys, M. Schuler, L.-P. Henry, and A. M. Läuchli, Observing the space- and time-dependent growth of correlations in dynamically tuned synthetic ising models with antiferromagnetic interactions, *Phys. Rev. X* **8**, 021070 (2018).
- [13] E. Guardado-Sanchez, P. T. Brown, D. Mitra, T. Devakul, D. A. Huse, P. Schauf, and W. S. Bakr, Probing the quench dynamics of antiferromagnetic correlations in a 2d quantum ising spin system, *Phys. Rev. X* **8**, 021069 (2018).
- [14] H. Kim, Y. Park, K. Kim, H.-S. Sim, and J. Ahn, Detailed balance of thermalization dynamics in rydberg-atom quantum simulators, *Phys. Rev. Lett.* **120**, 180502 (2018).
- [15] J. P. Garrahan, Aspects of non-equilibrium in classical and quantum systems: Slow relaxation and glasses, dynamical large deviations, quantum non-ergodicity, and open quantum dynamics, *Physica A: Statistical Mechanics and its Applications* **504**, 130 (2018).
- [16] M. Fruchart, R. Hanai, P. B. Littlewood, and V. Vitelli, Non-reciprocal phase transitions, *Nature* **592**, 363 (2021).
- [17] S. Shankar, A. Souslov, M. J. Bowick, M. C. Marchetti, and V. Vitelli, Topological active matter, *Nature Reviews Physics* **4**, 380 (2022).
- [18] S.-H. Wei, B. Jing, X.-Y. Zhang, J.-Y. Liao, C.-Z. Yuan, B.-Y. Fan, C. Lyu, D.-L. Zhou, Y. Wang, G.-W. Deng, *et al.*, Towards real-world quantum networks: a review, *Laser & Photonics Reviews* **16**, 2100219 (2022).
- [19] N. Pancotti, G. Giudice, J. I. Cirac, J. P. Garrahan, and M. C. Bañuls, Quantum east model: Localization, non-thermal eigenstates, and slow dynamics, *Phys. Rev. X* **10**, 021051 (2020).
- [20] R. J. Valencia-Tortora, N. Pancotti, and J. Marino, Kinetically constrained quantum dynamics in superconducting circuits, *PRX Quantum* **3**, 020346 (2022).
- [21] J. P. Garrahan, R. L. Jack, V. Lecomte, E. Pitard, K. van Duijvendijk, and F. van Wijland, First-order dynamical phase transition in models of glasses: an approach based on ensembles of histories, *Journal of Physics A: Mathematical and Theoretical* **42**, 075007 (2009).
- [22] P. Chleboun, A. Faggionato, and F. Martinelli, Time scale separation in the low temperature east model: rigorous results, *J. Stat. Mech.* **2013**, L04001 (2013).
- [23] Z. Lan, M. van Horssen, S. Powell, and J. P. Garrahan, Quantum slow relaxation and metastability due to dynamical constraints, *Phys. Rev. Lett.* **121**, 040603 (2018).
- [24] L. Causser, I. Lesanovsky, M. C. Bañuls, and J. P. Garrahan, Dynamics and large deviation transitions of the xor-fredrickson-andersen kinetically constrained model, *Phys. Rev. E* **102**, 052132 (2020).
- [25] C. J. Turner, A. A. Michailidis, D. A. Abanin, M. Serbyn, and Z. Papić, Weak ergodicity breaking from quantum many-body scars, *Nature Physics* **14**, 745 (2018).
- [26] S. Choi, C. J. Turner, H. Pichler, W. W. Ho, A. A. Michailidis, Z. Papić, M. Serbyn, M. D. Lukin, and D. A. Abanin, Emergent su(2) dynamics and perfect quantum many-body scars, *Phys. Rev. Lett.* **122**, 220603 (2019).
- [27] M. Serbyn, D. A. Abanin, and Z. Papić, Quantum many-body scars and weak breaking of ergodicity, *Nature Physics* **17**, 675 (2021).
- [28] C. J. Turner, A. A. Michailidis, D. A. Abanin, M. Serbyn, and Z. Papić, Quantum scarred eigenstates in a rydberg atom chain: Entanglement, breakdown of thermalization, and stability to perturbations, *Phys. Rev. B* **98**, 155134 (2018).
- [29] V. Khemani, C. R. Laumann, and A. Chandran, Signatures of integrability in the dynamics of rydberg-blockaded chains, *Phys. Rev. B* **99**, 161101 (2019).
- [30] C. J. Turner, J.-Y. Desaulès, K. Bull, and Z. Papić, Correspondence principle for many-body scars in ultracold rydberg atoms, *Phys. Rev. X* **11**, 021021 (2021).
- [31] M. Kormos, M. Collura, G. Takács, and P. Calabrese, Real-time confinement following a quantum quench to a non-integrable model, *Nature Physics* **13**, 246 (2017).
- [32] A. Lerose, F. M. Surace, P. P. Mazza, G. Peretto, M. Collura, and A. Gambassi, Quasilocalized dynamics from confinement of quantum excitations, *Phys. Rev. B* **102**, 041118 (2020).
- [33] M. Magoni, P. P. Mazza, and I. Lesanovsky, Emergent Bloch oscillations in a kinetically constrained rydberg spin lattice, *Phys. Rev. Lett.* **126**, 103002 (2021).
- [34] M. van Horssen, E. Levi, and J. P. Garrahan, Dynamics of many-body localization in a translation-invariant quantum glass model, *Phys. Rev. B* **92**, 100305 (2015).
- [35] I. Lesanovsky and J. P. Garrahan, Kinetic constraints, hierarchical relaxation, and onset of glassiness in strongly interacting and dissipative rydberg gases, *Phys. Rev. Lett.* **111**, 215305 (2013).
- [36] C. Pérez-Espigares, I. Lesanovsky, J. P. Garrahan, and R. Gutiérrez, Glassy dynamics due to a trajectory phase transition in dissipative rydberg gases, *Phys. Rev. A* **98**, 021804 (2018).
- [37] M. M. Valado, C. Simonelli, M. D. Hoogerland, I. Lesanovsky, J. P. Garrahan, E. Arimondo, D. Ciampini, and O. Morsch, Experimental observation of controllable kinetic constraints in a cold atomic gas, *Phys. Rev. A* **93**, 040701 (2016).
- [38] I. Lesanovsky and J. P. Garrahan, Out-of-equilibrium structures in strongly interacting rydberg gases with dissipation, *Phys. Rev. A* **90**, 011603 (2014).
- [39] D. Gribben, I. Lesanovsky, and R. Gutiérrez, Quench dynamics of a dissipative rydberg gas in the classical and quantum regimes, *Phys. Rev. A* **97**, 011603 (2018).
- [40] M. Ostmann, M. Marcuzzi, J. P. Garrahan, and I. Lesanovsky, Localization in spin chains with facilitation constraints and disordered interactions, *Phys. Rev. A* **99**, 060101 (2019).
- [41] M. Marcuzzi, J. c. v. Minář, D. Barredo, S. de Léséleuc, H. Labuhn, T. Lahaye, A. Browaeys, E. Levi, and I. Lesanovsky, Facilitation dynamics and localization phenomena in rydberg lattice gases with position disorder, *Phys. Rev. Lett.* **118**, 063606 (2017).
- [42] R. Nandkishore and D. A. Huse, Many-body localization and thermalization in quantum statistical mechanics, *Annual Review of Condensed Matter Physics* **6**, 15 (2015), <https://doi.org/10.1146/annurev-conmatphys-031214-014726>.
- [43] D. A. Abanin, E. Altman, I. Bloch, and M. Serbyn, Colloquium: Many-body localization, thermalization, and entanglement, *Rev. Mod. Phys.* **91**, 021001 (2019).

- [44] V. Khemani, M. Hermele, and R. Nandkishore, Localization from hilbert space shattering: From theory to physical realizations, *Phys. Rev. B* **101**, 174204 (2020).
- [45] S. Moudgalya and O. I. Motrunich, Hilbert space fragmentation and commutant algebras, *Phys. Rev. X* **12**, 011050 (2022).
- [46] M. Schulz, C. A. Hooley, R. Moessner, and F. Pollmann, Stark many-body localization, *Phys. Rev. Lett.* **122**, 040606 (2019).
- [47] E. V. H. Doggen, I. V. Gornyi, and D. G. Polyakov, Stark many-body localization: Evidence for hilbert-space shattering, *Phys. Rev. B* **103**, L100202 (2021).
- [48] W. Morong, F. Liu, P. Becker, K. S. Collins, L. Feng, A. Kyprianidis, G. Pagano, T. You, A. V. Gorshkov, and C. Monroe, Observation of stark many-body localization without disorder, *Nature* **599**, 393 (2021).
- [49] S. Scherg, T. Kohlert, P. Sala, F. Pollmann, B. H. Madhusudhana, I. Bloch, and M. Aidelsburger, Observing non-ergodicity due to kinetic constraints in tilted fermi-hubbard chains, *Nature Communications* **12**, 10.1038/s41467-021-24726-0 (2021).
- [50] D. Jaksch, J. I. Cirac, P. Zoller, S. L. Rolston, R. Côté, and M. D. Lukin, Fast quantum gates for neutral atoms, *Phys. Rev. Lett.* **85**, 2208 (2000).
- [51] C. Ates, T. Pohl, T. Pattard, and J. M. Rost, Many-body theory of excitation dynamics in an ultracold rydberg gas, *Phys. Rev. A* **76**, 013413 (2007).
- [52] Supplemental material with the details about the numerical methods, derivation of the effective theories, and discussion on classical rate equations.
- [53] M. Ostmann, M. Marcuzzi, J. Minář, and I. Lesanovsky, Synthetic lattices, flat bands and localization in rydberg quantum simulators, *Quantum Science and Technology* **4**, 02LT01 (2019).
- [54] S. Moudgalya, B. A. Bernevig, and N. Regnault, Quantum many-body scars and hilbert space fragmentation: a review of exact results, *Reports on Progress in Physics* **85**, 086501 (2022).
- [55] F. Balducci, A. Gambassi, A. Lerose, A. Scardicchio, and C. Vanoni, Interface dynamics in the two-dimensional quantum ising model, *Phys. Rev. B* **107**, 024306 (2023).
- [56] G. H. Wannier, Wave functions and effective hamiltonian for bloch electrons in an electric field, *Phys. Rev.* **117**, 432 (1960).
- [57] G. H. Wannier, Dynamics of band electrons in electric and magnetic fields, *Rev. Mod. Phys.* **34**, 645 (1962).
- [58] F. Liu, R. Lundgren, P. Titum, G. Pagano, J. Zhang, C. Monroe, and A. V. Gorshkov, Confined quasiparticle dynamics in long-range interacting quantum spin chains, *Phys. Rev. Lett.* **122**, 150601 (2019).
- [59] V. Lienhard, P. Scholl, S. Weber, D. Barredo, S. de Léséleuc, R. Bai, N. Lang, M. Fleischhauer, H. P. Büchler, T. Lahaye, and A. Browaeys, Realization of a density-dependent peierls phase in a synthetic, spin-orbit coupled rydberg system, *Phys. Rev. X* **10**, 021031 (2020).
- [60] G. H. Fredrickson and H. C. Andersen, Kinetic ising model of the glass transition, *Phys. Rev. Lett.* **53**, 1244 (1984).
- [61] M. Fishman, S. R. White, and E. M. Stoudenmire, The ITensor Software Library for Tensor Network Calculations, *SciPost Phys. Codebases* , 4 (2022).
- [62] J. Gray, quimb: A python package for quantum information and many-body calculations, *Journal of Open Source Software* **3**, 819 (2018).

## SUPPLEMENTAL MATERIAL

### Numerical simulations

Results in Fig. 1(c-d) were obtained via tensor network methods using the C++ version of the ITensor library [61]. Specifically, we performed the time evolution via a 3-sites Time Evolving Block Decimation (TEBD) algorithm setting a maximal bond dimension  $\chi_{\max} = 500$  (well above what dynamically reached) and timestep  $\delta t = 10^{-3}$ . All the other results were obtained via exact diagonalization using the Python package quimb [62].

### Alternative scheme for obtaining directional antiblockade condition

Here we discuss a different, but equivalent, route for obtaining the *directional* antiblockade condition. Given Eq. (1), we set again  $\Omega_2 = 0$  as it is not necessary for this purpose. In the main text, we discussed a scheme based on a staggered configuration in the atomic distances and drive field frequencies driving the atoms. Here, we retain the essential ingredient of a staggered configuration in the atomic spacings. However, instead of imprinting the staggered configuration on the drive field frequencies, which we set to be homogeneous in space, we impose the staggered configuration on the atomic transition frequencies. This condition could be achieved by site-resolved magnetic fields. Specifically, we set the atomic transition frequencies to be detuned by  $-V_1$  from the drive field when  $j$  is even and by  $-V_2$  when  $j$  is odd. In this manner, the *directional* antiblockade condition discussed in the main text emerges, as the drive field acting on the  $j$ -th atom is resonant only when the  $(j-1)$ -th atom is excited. This can be seen explicitly writing the Hamiltonian in the rotating frame with respect to the drive field, which is given by

$$\hat{H} = -\sum_{j=1}^N V_{j-1,j} \hat{n}_j + \frac{\Omega_1}{2} \sum_{j=1}^N \hat{\sigma}_j^x + V_1 \sum_{j \text{ odd}} \hat{n}_j \hat{n}_{j+1} + V_2 \sum_{j \text{ even}} \hat{n}_j \hat{n}_{j+1} + V_{\text{NNN}} \sum_{j=1}^{N-2} \hat{n}_j \hat{n}_{j+2}. \quad (5)$$

From Eq. (5), it can be seen that if the  $(j-1)$ -th is excited, the energy shift cancels the contribution from the first term on the  $j$ -th atom, making the acting drive field resonant and able to induce a spin-flip.

### Derivation of effective theory with both sets of drive fields

Given the Hamiltonian in Eq. (1), we set  $\Omega_{1,j}(t) = \Omega_1 e^{-i(V_{j-1,j}-\epsilon)t}$  and  $\Omega_2(t) = \Omega_2 e^{-i(V_1+V_2-\epsilon)t}$ , obtaining

$$\hat{H}(t) = \sum_{j=1}^N \left[ \frac{1}{2} \left( \Omega_1 e^{-i(V_{j-1,j}-\epsilon)t} + \Omega_2 e^{-i(V_1+V_2-\epsilon)t} \right) \hat{\sigma}_j^+ + \text{H.c.} \right] + V_1 \sum_{j \text{ odd}} \hat{n}_j \hat{n}_{j+1} + V_2 \sum_{j \text{ even}} \hat{n}_j \hat{n}_{j+1} + V_{\text{NNN}} \sum_{j=1}^{N-2} \hat{n}_j \hat{n}_{j+2}, \quad (6)$$

In order to obtain the effective Hamiltonian, we pass in interaction picture  $\hat{H}_{\text{int}} = \hat{U}^\dagger \hat{H} \hat{U} - \hat{H}_0$  with

$$\hat{U} = \exp \left[ -i \hat{H}_0 t \right], \quad \hat{H}_0 = -\epsilon \sum_{j=1}^N \hat{n}_j + \sum_{j=1}^{N-1} V_{j,j+1} n_j n_{j+1}. \quad (7)$$

We have

$$e^{-i\epsilon \sum_j \hat{n}_j t} \hat{\sigma}_j^+ e^{i\epsilon \sum_j \hat{n}_j t} = e^{-i\epsilon |1\rangle \langle 1| t} |1\rangle \langle 0| e^{i \sum_j \Delta_j |1\rangle \langle 1| t} = e^{-i\epsilon t} \hat{\sigma}_j^+, \quad (8)$$

and, exploiting  $\hat{n}_i^k = \hat{n}_i$  for  $k \in \mathbb{N}^+$ , we have

$$\begin{aligned} e^{+i \sum_j V_{j-1,j} \hat{n}_{j-1} \hat{n}_j t} \hat{\sigma}_i^+ e^{-i \sum_j V_{j-1,j} \hat{n}_{j-1} \hat{n}_j t} &= e^{+i V_{i-1,i} \hat{n}_{i-1} t} \hat{\sigma}_i^+ e^{+i V_{i,i+1} \hat{n}_{i+1} t} \\ &= \left[ 1 + \left( \sum_{k=1}^{\infty} \frac{(i V_{i-1,i} t)^k}{k!} \right) \hat{n}_{i-1} \right] \hat{\sigma}_i^+ \left[ 1 + \left( \sum_{k=1}^{\infty} \frac{(i V_{i,i+1} t)^k}{k!} \right) \hat{n}_{i+1} \right] \\ &= [1 + (e^{+i V_{i-1,i} t} - 1) \hat{n}_{i-1}] \hat{\sigma}_i^+ [1 + (e^{+i V_{i,i+1} t} - 1) \hat{n}_{i+1}] \\ &= \left( \hat{P}_{i-1} + e^{+i V_{i-1,i} t} \hat{n}_{i-1} \right) \hat{\sigma}_i^+ \left( \hat{P}_{i+1} + e^{+i V_{i,i+1} t} \hat{n}_{i+1} \right) \end{aligned} \quad (9)$$



where we have introduced  $\hat{P}_i = (1 - \hat{n}_i)$  (projector on the vacuum). Thus, paying attention to the boundary terms, the Hamiltonian in interaction picture is given by

$$\begin{aligned} \hat{H}_{\text{int}} = & \frac{1}{2} \left\{ \left( \Omega_1 e^{-iV_2 t} + \Omega_2 e^{-i(V_1+V_2)t} \right) \hat{\sigma}_1^+ \left( \hat{P}_2 + e^{+iV_1 t} \hat{n}_2 \right) + H.c. \right\} + \\ & + \frac{1}{2} \sum_{j=2}^{N-1} \left\{ \left( \Omega_1 e^{-iV_{j-1,j} t} + \Omega_2 e^{-i(V_1+V_2)t} \right) \left( \hat{P}_{j-1} + e^{+iV_{j-1,j} t} \hat{n}_{j-1} \right) \hat{\sigma}_j^+ \left( \hat{P}_{j+1} + e^{+iV_{j,j+1} t} \hat{n}_{j+1} \right) + H.c. \right\} + \\ & + \frac{1}{2} \left\{ \left( \Omega_1 e^{-iV_{N-1,N} t} + \Omega_2 e^{-i(V_1+V_2)t} \right) \left( \hat{P}_{N-1} + e^{+iV_{N-1,N} t} \hat{n}_{N-1} \right) \hat{\sigma}_N^+ + H.c. \right\} + \\ & + \epsilon \sum_{j=1}^N \hat{n}_j + V_{\text{NNN}} \sum_{j=1}^{N-2} \hat{n}_j \hat{n}_{j+2}. \end{aligned} \quad (10)$$

Given Eq. (10), we obtain the effective theory in Eq. (2) of the main text applying the RWA in the limit  $|V_1 - V_2|, V_{1,2} \gg |\Omega_{1,2}|$ , keeping the most resonant processes (the ones without any time dependence).

### Effective Hamiltonian for $\Omega_2 = 0$

When  $\Omega_2 = 0$ , the number of strings of excitations  $\hat{Q} = \sum_j \hat{n}_j (1 - \hat{n}_{j+1})$  commutes with the Hamiltonian. Additionally, due to the ‘East symmetry’, the left edge of each string does not move. As a consequence, the dynamics of a  $\mathcal{N}$ -strings state can be computed from the dynamics of  $\mathcal{N}$  1-string states. Therefore, we can focus on the symmetry sector with a single string ( $Q = 1$ ). A complete basis of single-kink states is given by  $|\mathbf{k}\rangle = \bigotimes_{j=1}^k |1\rangle \bigotimes_{j=k+1}^N |0\rangle$ . Given

$$\begin{aligned} \langle \mathbf{q} | \hat{n}_j \hat{n}_{j+2} | \mathbf{k} \rangle &= \delta_{q,k} \theta(k - (j + 2)), \\ \langle \mathbf{q} | \hat{n}_j \hat{\sigma}_{j+1}^x | \mathbf{k} \rangle &= \delta_{q-1,k} \delta_{j-1,k} + \delta_{q+1,k} \delta_{j,k}, \\ \langle \mathbf{q} | \hat{n}_j \hat{\sigma}_{j+1}^x \hat{n}_{j+2} | \mathbf{k} \rangle &= 0, \end{aligned} \quad (11)$$

and plugging them in the Hamiltonian in Eq. (2) represented in the same basis

$$\hat{H} = \sum_{k,q} \langle \mathbf{q} | \hat{H} | \mathbf{k} \rangle | \mathbf{q} \rangle \langle \mathbf{k} |, \quad (12)$$

we straightforwardly obtain Eq. (3).

### Classical rate equations

Let us restrict for simplicity to the single drive field regime setting  $\Omega_2 = 0$ . We keep the detuning  $\Delta_j$  of the drive field frequency from the bare atomic transition as a free parameter for generality. In the rotating frame with respect to the drive fields, the starting Hamiltonian is given by

$$\hat{H} = \sum_{j=1}^N \Delta_j \hat{n}_j + \frac{\Omega}{2} \sum_{j=1}^N \hat{\sigma}_j^x + \frac{1}{2} \sum_{i,j} V_{i,j} \hat{n}_i \hat{n}_j. \quad (13)$$

Due to the presence of dephasing, the full dynamics of the state  $\hat{\rho}$  is given by the Lindblad master equation

$$\partial_t \hat{\rho} = -i[\hat{H}, \hat{\rho}] + \gamma \sum_j \left( \hat{n}_j \hat{\rho} \hat{n}_j - \frac{1}{2} \{ \hat{n}_j, \hat{\rho} \} \right) \quad (14)$$

In the main text we have worked in the regime  $\gamma \ll \Omega$ . Now, we work in the opposite regime  $\gamma \gg \Omega$ . In this regime, we can distinguish fast and slow processes: the fast processes are controlled by the interacting part of the Hamiltonian and the dissipative process; the slow processes are controlled by the external drive fields. Projecting out the fast dynamics (see Ref. [35] for the derivation), the dynamics of the projected state  $\hat{\mu}$  is governed by

$$\partial_t \hat{\mu} = \frac{4\Omega^2}{\gamma} \sum_j \Gamma_j \left( \hat{\sigma}_j^x \hat{\mu} \hat{\sigma}_j^x - \hat{\mu} \right), \quad (15)$$

with rates dependent on the parameters of the Hamiltonian, dissipation and atomic configuration

$$\Gamma_j^{-1} = 1 + 4 \left( \frac{\Delta_j + \sum_{m \neq j} V_{j,m} \hat{n}_m}{\gamma} \right)^2. \quad (16)$$

Let us focus on a specific site  $j$  and fix the staggered configuration in the potentials discussed in the main text. Keeping up to nearest-neighbour terms, the rate in Eq. (16) turns into

$$\Gamma_j^{-1} = 1 + 4 \left( \frac{\Delta_j + V_1 \hat{n}_{j-1} + V_2 \hat{n}_{j+1}}{\gamma} \right)^2, \quad (17)$$

where we have assumed  $V_{j-1,j} = V_1$  and  $V_{j,j+1} = V_2$ , without losing generality. As evident, the rate  $\Gamma_j$  depends on the atomic configuration and  $\Delta_j$ . We aim to show that the rates are not symmetric under exchange of the pair of excitations  $(j-1) \leftrightarrow (j+1)$ . To do so, in Fig. 4(a) we show the rate as a function of  $\Delta_j$  for  $V_2 = 2 \times V_1$  in the non-symmetric scenarios, namely  $n_{j-1} = 1, n_{j+1} = 0$  and viceversa. It is evident that at fixed parameters, the rates is generally not symmetric as desired for  $V_1 \neq V_2$  (except for a fine tuned value of  $\Delta_j$  at which the curves cross). As in the coherent case, the degree of directionality can be tuned via  $|V_1 - V_2|$  and  $\Delta$  (cf. Fig. 4(b)).

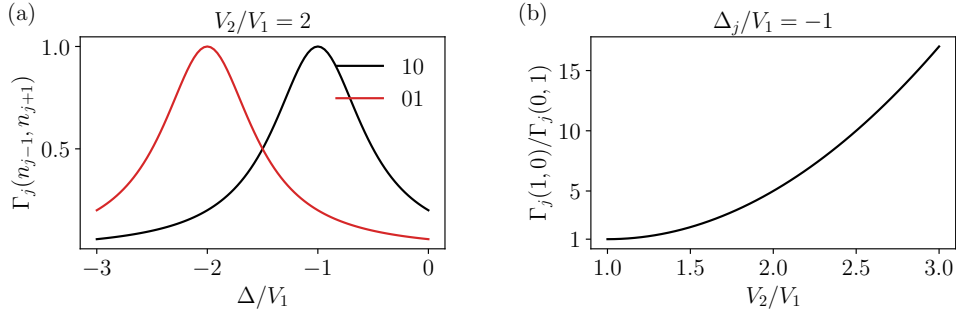


FIG. 4. (a) Rate  $\Gamma_j$  (cf. Eq. (17)) at fixed  $V_2/V_1 = 2$  and atomic configurations (values of  $n_{j-1}$  and  $n_{j+1}$ ). As evident, the rate is not symmetric under exchange of the neighbouring atoms (the two curves do not overlap). (b) Ratio of the rates  $\Gamma_j$  in the two scenario  $n_{j-1} = 1, n_{j+1} = 0$  and viceversa at fixed  $\Delta_j = -V_1$ . In the symmetric case ( $V_1 = V_2$ ) no notion of directionality appears ( $\Gamma_j(1,0)/\Gamma_j(0,1) = 1$ ). Instead, for  $V_1 \neq V_2$ , rates display ‘chiral’ features ( $\Gamma_j(1,0)/\Gamma_j(0,1) \neq 1$ ). The ‘chirality’ can be readily tuned by simply changing the ratio  $V_1/V_2$ , or the detuning  $\Delta_j$ . In all the calculations we have set  $\gamma/V_1 = 1$ .